Article:
Wang, W., Chen, H. orcid.org/0000-0002-2918-8735, Liu, W. orcid.org/0000-0003-2968-2888 et al. (2 more authors) (2023) Trilinear decomposition based near-field source localization with MIMO velocity vector sensor arrays. Signal Processing, 210. 109061. ISSN 0165-1684

https://doi.org/10.1016/j.sigpro.2023.109061

Trilinear Decomposition Based Near-Field Source Localization with MIMO Velocity Vector Sensor Arrays

Weilong Wang[a], Hua Chen[a,b,*], Wei Liu[c], Qing Wang[d], Gang Wang[a,b]

[a]*Faculty of Electrical Engineering and Computer Science, Ningbo University, Ningbo 315211, P. R. China.*
[b]*Zhejiang Key Laboratory of Mobile Network Application Technology, Ningbo 315211, P. R. China.*
[c]*Department of Electronic and Electrical Engineering, University of Sheffield, Sheffield S1 3JD, UK.*
[d]*School of Electronic Informatin Engineering, Tianjin University, Tianjin 300072, P. R. China.*

Abstract

This paper studies the near-field (NF) parameter estimation problem for a multiple-input multiple-output (MIMO) array system, which employs multiple pairs of orthogonal velocity sensors at both the transmitter and the receiver. A trilinear decomposition method is proposed to estimate the four-dimensional (4-D) parameters, including the direction of departure (DOD), the range from transmitter to target (RFTT), the direction of arrival (DOA), and the range from target to receiver (RFTR). Firstly, the output of the matched filter at the receiver is formulated in a third-order parallel factor (PARAFAC) model; secondly, the initial coarse estimates of DOD, RFTT, DOA and RFTR embedded in the velocity vector sensors are obtained through trilinear decomposition, and then more accurate estimates of DOD,

*Corresponding author
Email addresses: dkchenhua0714@hotmail.com (Hua Chen), w.liu@sheffield.ac.uk (Wei Liu), wqelaine@tju.edu.cn (Qing Wang), wanggang@nbu.edu.cn (Gang Wang)

RFTT, DOA and RFTR are achieved from the steering vector. The proposed method is search-free and has a close form, with automatically paired results. Its performance is demonstrated via numerical examples.
Keywords: MIMO, velocity vector sensor, near-field, parallel factor.

1. Introduction

In the past few decades, many efforts have been devoted to acoustic vector sensor signal processing, which now has been widely used in underwater communication, surveillance and other similar fields [1, 2]. Either a complete (four-component) acoustic vector sensor including three orthogonal velocity sensors plus an isotropic pressure sensor, or an incomplete (two-, three-component) one can be employed for localization and tracking [3–5]. A representative localization method using a complete acoustic vector sensor array is proposed in [6], along with the Cramer-Rao bound (CRB) derived as a benchmark. For an incomplete one, a successive multiple signal classification (MUSIC) method for a multi-input multi-output (MIMO) array system with multiple pairs of velocity receive sensors is proposed in [7], which uses the direction of arrival (DOA) information embedded in the velocity sensors to perform two consecutive one-dimensional (1-D) MUSIC searches for direction of departure (DOD) and DOA in turn. Further, with the same MIMO system, an improved dimensionality-reduction MUSIC algorithm is proposed to estimate the DOD and DOA [8] , which only requires a local 1-D search to obtain the DOA estimate, and then the least squares principle is adopted to obtain the DOD estimates. In order to avoid spectral peak search, an extended unitary root MUSIC algorithm is proposed in [9] for a sparse nested

MIMO radar system with velocity receiver sensors, which can obtain a larger aperture and achieve better DOA estimation performance. However, none of the above three methods considers velocity diversity in the transmitter, which underutilizes the wealth of information on MIMO arrays and velocity arrays, and more importantly they cannot be applied to near-field (NF) source localization directly.

Several NF source localization methods [10–12] have been presented based on one acoustic vector sensor with a satisfactory performance achieved; however, they are only focused on the receiver side. In this paper, a four-dimensional (4-D) parameter estimation method for a bistatic MIMO system is proposed, where both the transmitter and the receiver are equipped with velocity vector sensor arrays. Trilinear decomposition is performed to obtain the initial coarse estimates of DOD, DOA, the range from transmitter to target (RFTT) and the range from target to receiver (RFTR), based on which, more accurate estimates of DOD, DOA, RFTT and RFTR are then derived with the steering vector. The proposed method avoids spectral peak search, and the associated 4-D parameters can be automatically paired. Note that an ideal model is adopted in this work and more practical factors need to be considered in the future. For example, the amplitude of the received signal may vary from sensor to sensor and be inversely proportional to the source-sensor distance, as pointed out in [13, 14]; the acoustic propagation environment may include the effects of turbulence, medium convection, temperature gradient, and pressure gradient, etc. Further work is needed for more practical models.

Notations: $(\cdot)^{-1}$, $(\cdot)^T$, $(\cdot)^\dagger$ and $(\cdot)^H$ represent inverse, transpose, pseudo-

inverse, and conjugate transpose, respectively; $\mathbf{I}_p$ stands for the $p \times p$ identity matrix; $\otimes$, $\odot$ and $\oplus$ are the Kronecker product, Khatri-Rao product and Hadamard product, respectively; $\mathbf{1}_p$ represents an all-one $p \times 1$ column vector; $\|\cdot\|_F$ is the Frobenius norm; $Re\{\cdot\}$ denotes taking real part operation; $\angle$ indicates the phase information; $|\cdot|$ represents the absolute value.

2. Signal Model

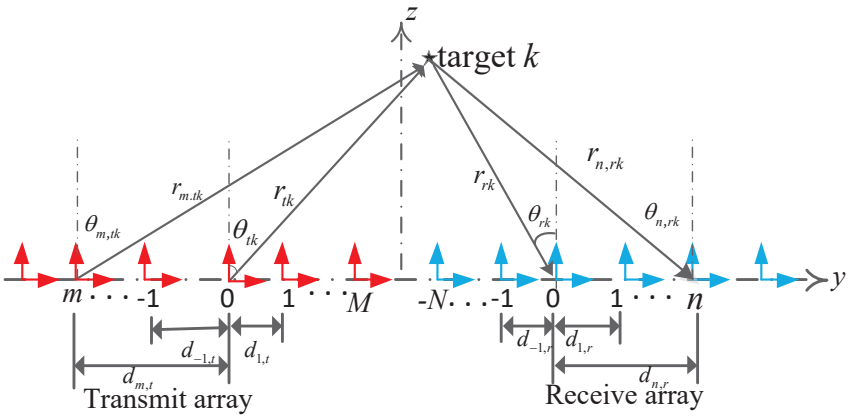

Figure 1: Geometry of the considered MIMO velocity vector sensor arrays.

Consider a bistatic MIMO system equipped with a nonuniform linear array (NULA) of $2M+1$ and $2N+1$ vector sensors at the transmitter and the receiver, respectively, as shown in Fig. 1. Take the center of the transmitting and receiving arrays as the reference point, respectively. Each array element consists of a pair of velocity sensors, which are aligned with the y-axis and the z -axis, respectively. Let $d_{m,t}$ and $d_{n,r}$ represent the range between the m-th transmit sensor and the reference transmit sensor, the range between the

n-th receiver sensor and the reference receive sensor. Assume that there are K NF targets located on the yoz plane, parametrized by the DOD, DOA, RFTT and RFTR and denoted as θ_{tk}, θ_{rk}, r_{tk} and r_{rk}, respectively, with $k = 1, \cdots, K$. The unit velocity vectors at the mth transmit and nth receive sensors towards the kth NF target are respectively given by [6]

$$\mathbf{c}_{m,tk} = [\sin\theta_{m,tk}, \cos\theta_{m,tk}]^T \tag{1}$$

$$\mathbf{c}_{n,rk} = [\sin\theta_{n,rk}, \cos\theta_{n,rk}]^T \tag{2}$$

where $\theta_{m,tk} = \cos^{-1}\left(\frac{r_{tk}\cos\theta_{tk}}{\sqrt{r_{tk}^2+d_{m,t}^2-2r_{tk}d_{m,t}\sin\theta_{tk}}}\right)$ and $\theta_{n,rk} = \cos^{-1}\left(\frac{r_{rk}\cos\theta_{rk}}{\sqrt{r_{rk}^2+d_{n,r}^2+2r_{rk}d_{n,r}\sin\theta_{rk}}}\right)$ with $\theta_{0,tk} = \theta_{tk}$, $\theta_{0,rk} = \theta_{rk}$, $m = -M, \cdots, 0, \cdots, M$ and $n = -N, \cdots, 0, \cdots, N$.

Then, the output data of the receive velocity vector sensors at time t, after matched filtering, can be expressed as

$$\mathbf{y}(t) = (\mathbf{A}_t \odot \mathbf{A}_r)\mathbf{s}(t) + \mathbf{n}(t) \tag{3}$$

where $\mathbf{s}(t)$ denotes the reflected coefficient vector and $\mathbf{n}(t)$ is the complex additive white Gaussian noise with zero mean and a variance of σ_n^2. $\mathbf{A}_t = [\mathbf{a}_{t1}(\theta_{t1}, r_{t1}), \cdots, \mathbf{a}_{tK}(\theta_{tK}, r_{tK})]$ and $\mathbf{A}_r = [\mathbf{a}_{r1}(\theta_{r1}, r_{r1}), \cdots, \mathbf{a}_{rK}(\theta_{rK}, r_{rK})]$ are the steering vectors of the transmitting array and the receiving array, respectively, with each column denoted as

$$\mathbf{a}_{tk}(\theta_{tk}, r_{tk}) = [\mathbf{b}_{-M,tk}^T, \cdots, \mathbf{b}_{0,tk}^T, \cdots, \mathbf{b}_{M,tk}^T]^T \tag{4}$$

$$\mathbf{a}_{rk}(\theta_{rk}, r_{rk}) = [\mathbf{b}_{-N,rk}^T, \cdots, \mathbf{b}_{0,rk}^T, \cdots, \mathbf{b}_{N,,rk}^T]^T \tag{5}$$

where $\mathbf{b}_{m,tk} = \mathbf{c}_{m,tk}e^{j\tau_{m,tk}}$ and $\mathbf{b}_{n,rk} = \mathbf{c}_{n,rk}e^{j\tau_{n,rk}}$ with the phase factor

$$\begin{aligned}\tau_{m,tk} &= \frac{2\pi}{\lambda}(r_{m,tk} - r_{tk}) \\ &= \frac{2\pi}{\lambda}\left(\sqrt{r_{tk}^2 + d_{m,t}^2 - 2r_{tk}d_{m,t}\sin\theta_{tk}} - r_{tk}\right)\end{aligned} \tag{6}$$

$$\begin{aligned}\tau_{n,rk} &= \frac{2\pi}{\lambda}\left(r_{n,rk} - r_{rk}\right) \\ &= \frac{2\pi}{\lambda}\left(\sqrt{r_{rk}^2 + d_{n,r}^2 - 2r_{rk}d_{n,r}\sin\theta_{rk}} - r_{rk}\right)\end{aligned} \tag{7}$$

By collecting L snapshots, the observation of the receive array can be expressed as

$$\begin{aligned}\mathbf{Y} &= \begin{bmatrix} \mathbf{Y}_1 \\ \mathbf{Y}_2 \\ \vdots \\ \mathbf{Y}_{2(2N+1)} \end{bmatrix} = \begin{bmatrix} \mathbf{A}_t\mathbf{D}_1(\mathbf{A}_r) \\ \mathbf{A}_t\mathbf{D}_2(\mathbf{A}_r) \\ \vdots \\ \vdots \\ \mathbf{A}_t\mathbf{D}_{2(2N+1)}(\mathbf{A}_r) \end{bmatrix}\mathbf{S}^T + \mathbf{N}_y \\ &= (\mathbf{A}_t \odot \mathbf{A}_r)\mathbf{S}^T + \mathbf{N}_y\end{aligned} \tag{8}$$

where $\mathbf{D}_i(\cdot)$ represents the diagonal matrix formed by taking the ith row of a matrix, $\mathbf{S} = [\mathbf{s}(1), \mathbf{s}(2), \cdots, \mathbf{s}(L)]$ is the reflected coefficient matrix of size $K \times L$, $\mathbf{N}_y = [\mathbf{n}(1), \mathbf{n}(2), \cdots, \mathbf{n}(L)]$ is the signal noise of L snapshots, and $\mathbf{Y}_i = \mathbf{A}_t\mathbf{D}_i(\mathbf{A}_r)\mathbf{S}^T + \mathbf{N}_{yi}$, $i = 1, 2, \cdots, 2(2N+1)$, with $\mathbf{N}_{yi}$ being the ith slice of noise.

Additionally, $\mathbf{Y}_i$ can also be expressed in the following trilinear model

$$y_{i,p,j} = \sum_{k=1}^{K} a_{i,tk}a_{p,rk}s_{j,k} + n_{i,p,j} \tag{9}$$

where $a_{i,tk}$ and $a_{p,rk}$ are the (i,k) and (p,k) elements of $\mathbf{A}_t$ and $\mathbf{A}_r$, respectively, $s_{j,k}$ is the (j,k) element of $\mathbf{S}$, and $n_{i,p,j}$ is the (p,j) element of $\mathbf{N}_{xi}$. According to the structural feature of the PARAFAC model, (8) can also be represented in two other slice forms

$$\mathbf{X} = (\mathbf{A}_r \odot \mathbf{S})\mathbf{A}_t^T + \mathbf{N}_x \tag{10}$$

$$\mathbf{Z} = (\mathbf{S} \odot \mathbf{A}_t)\mathbf{A}_r^T + \mathbf{N}_z. \tag{11}$$

3. Proposed Method

3.1. Trilinear Decomposition

According to (8), the least squares (LS) fit can be denoted as

$$\min_{\mathbf{A}_t,\mathbf{A}_r,\mathbf{S}} \parallel \mathbf{Y} - (\mathbf{A}_t \odot \mathbf{A}_r)\mathbf{S}^T\parallel_F. \tag{12}$$

Then, the LS update of $\mathbf{S}$ is given by

$$\hat{\mathbf{S}}^T = (\hat{\mathbf{A}}_t^T \odot \hat{\mathbf{A}}_r^T)^\dagger \mathbf{Y} \tag{13}$$

where $\hat{\mathbf{A}}_t$ and $\hat{\mathbf{A}}_r$ are the corresponding estimates of $\mathbf{A}_t$ and $\mathbf{A}_r$ obtained from the previous iteration.

Similarly, the LS fitting of (10) can be expressed as

$$\min_{\mathbf{A}_t,\mathbf{A}_r,\mathbf{S}} \parallel \mathbf{X} - (\mathbf{A}_r \odot \mathbf{S})\mathbf{A}_t^T\parallel_F. \tag{14}$$

Then, the LS solution for $\mathbf{A}_t$ is updated as

$$\hat{\mathbf{A}}_t^T = (\hat{\mathbf{A}}_r \odot \hat{\mathbf{S}})^\dagger \mathbf{X} \tag{15}$$

where $\hat{\mathbf{A}}_r$ and $\hat{\mathbf{S}}$ are the estimates of $\mathbf{A}_r$ and $\mathbf{S}$ obtained from the previous iteration.

From (11), the LS fitting can be obtained as

$$\min_{\mathbf{A}_t,\mathbf{A}_r,\mathbf{S}} \parallel \mathbf{Z} - (\mathbf{S} \odot \mathbf{A}_t)\mathbf{A}_r^T\parallel_F. \tag{16}$$

Then, the LS solution for $\mathbf{A}_r$ is updated as

$$\hat{\mathbf{A}}_r^T = (\hat{\mathbf{S}} \odot \hat{\mathbf{A}}_t)^\dagger \mathbf{Z} \tag{17}$$

where $\hat{\mathbf{S}}$ and $\hat{\mathbf{A}}_t$ are the estimates of $\mathbf{A}_r$ and $\mathbf{S}$ obtained from the previous iteration.

According to (13), (15) and (17), $\hat{\mathbf{S}}$, $\hat{\mathbf{A}}_t$ and $\hat{\mathbf{A}}_r$ are updated sequentially, and the process is repeated until the predefined convergence criterion is satisfied, and then estimates of the matrices $\mathbf{S}$, $\mathbf{A}_t$ and $\mathbf{A}_r$ can be obtained. The uniqueness of trilinear decomposition is supported by the following theorem [15].

Theorem [15]: Consider a trilinear model $\mathbf{Y}_i = \mathbf{A}_t\mathbf{D}_i(\mathbf{A}_r)\mathbf{S}^T$, $i = 1, 2, \cdots, 2(2N+1)$, where $\mathbf{A}_t \in \mathbf{C}^{2(2M+1)\times K}$, $\mathbf{A}_r \in \mathbf{C}^{2(2N+1)\times K}$, and $\mathbf{S} \in C^{L\times K}$. Provided that the ranks of the three matrices are $K_{\mathbf{A}_t}$, $K_{\mathbf{A}_r}$ and $K_{\mathbf{S}}$, respectively, which meet the following requirement

$$K_{\mathbf{A}_t} + K_{\mathbf{A}_r} + K_{\mathbf{S}} \geq 2K + 2, \tag{18}$$

$\mathbf{A}_t$, $\mathbf{A}_r$ and $\mathbf{S}$ are unique for column transformation and scaling transformation.

3.2. Coarse Parameter Estimation

After normalizing $\hat{\mathbf{A}}_t$, and according to definitions of $\mathbf{A}_t$ and $\mathbf{a}_{tk}$, the estimate of $\mathbf{b}_{m,tk}$ can be denoted as $\hat{\mathbf{b}}_{m,tk} = \hat{\mathbf{A}}_t(2m+2M+1 : 2m+2M+2, k)$, $m = -M, \cdots, 0, \cdots, M$, $k = 1, \cdots, K$. Then, $\theta_{m,tk}$ can be estimated via

$$\hat{\theta}_{m,tk} = \tan^{-1}\left(\frac{\hat{\mathbf{b}}_{m,tk}(1)}{\hat{\mathbf{b}}_{m,tk}(2)}\right), \tag{19}$$

Consequently, a coarse estimate of θ_{tk} is given by $\hat{\theta}_{tk}^{coa} = \hat{\theta}_{0,tk}$.

Thereafter, with the estimated $\hat{\theta}_{m,tk}$ and the geometric relationship in conjunction with Fig. 1, the coarse estimate of r_{tk} is given by

$$\hat{r}_{tk}^{coa} = \frac{\sum_{m=-M}^{-1}\left|\frac{d_{m,t}\cos\hat{\theta}_{m,tk}}{\sin(\hat{\theta}_{tk}^{coa}-\hat{\theta}_{m,tk})}\right| + \sum_{m=1}^{M}\left|\frac{d_{m,t}\cos\hat{\theta}_{m,tk}}{\sin(\hat{\theta}_{m,tk}-\hat{\theta}_{tk}^{coa})}\right|}{2M}. \tag{20}$$

Similar to (19), $\theta_{n,rk}$ can be estimated via

$$\hat{\theta}_{n,rk} = \tan^{-1}\left(\frac{\hat{\mathbf{b}}_{n,rk}(1)}{\hat{\mathbf{b}}_{n,rk}(2)}\right), \tag{21}$$

and thus, the coarse estimate of θ_{rk} is given by $\hat{\theta}_{rk}^{coa} = \hat{\theta}_{0,rk}$, and the coarse estimate of r_{rk} is

$$\hat{r}_{rk}^{coa} = \frac{\sum_{n=-N}^{-1}\left|\frac{d_{n,r}\cos\hat{\theta}_{n,rk}}{\sin(\hat{\theta}_{rk}^{coa}-\hat{\theta}_{n,rk})}\right| + \sum_{n=1}^{N}\left|\frac{d_{n,r}\cos\hat{\theta}_{n,rk}}{\sin(\hat{\theta}_{n,rk}-\hat{\theta}_{rk}^{coa})}\right|}{2N}. \tag{22}$$

3.3. Fine Parameter Estimation

Different from (19)-(22) for calculating the estimates of DOD, DOA, RFTT and RFTR embedded in the velocity vector sensors, the 4-D parameters can be obtained from the spatial phase factor $q_{m,tk} \triangleq e^{j\tau_{m,tk}}$ and $q_{n,rk} \triangleq e^{j\tau_{n,rk}}$, respectively. Therefore, we first calculate the estimates of $q_{m,tk}$ and $q_{n,rk}$ as follows

$$\hat{q}_{m,tk} = \begin{cases} 1, m = 0 \\ \frac{\hat{\mathbf{c}}_{0,tk}^T \hat{\mathbf{b}}_{m,tk}}{\hat{\mathbf{c}}_{m,tk}^T \hat{\mathbf{b}}_{0,tk}}, m \neq 0 \end{cases} \tag{23}$$

$$\hat{q}_{n,rk} = \begin{cases} 1, n = 0 \\ \frac{\hat{\mathbf{c}}_{0,rk}^T \hat{\mathbf{b}}_{n,rk}}{\hat{\mathbf{c}}_{n,rk}^T \hat{\mathbf{b}}_{0,rk}}, n \neq 0 \end{cases} \tag{24}$$

where $\hat{\mathbf{c}}_{m,tk}$ and $\hat{\mathbf{c}}_{n,rk}$ are the estimates of (1) and (2) obtained by exploiting the results of (19) and (21), respectively.

Obviously, if the inter-element spacing is less than one-quarter wavelength, the spatial phases of $\hat{q}_{m,tk}$ and $\hat{q}_{n,rk}$ are unambiguous. However, when the inter-element spacing is more than one-quarter wavelength, the spatial phase obtained directly from $\hat{q}_{m,tk}$ and $\hat{q}_{n,rk}$ will be ambiguous. In this case, we first need to obtain the unambiguous spatial phase.

According to earlier discussion, θ_{tk}^{coa}, r_{tk}^{coa}, θ_{rk}^{coa} and r_{rk}^{coa} are unambiguous since they are estimated for the velocity vectors. With the coarse estimates of the 4-D parameters, the coarse but unambiguous spatial phase factors $\tau_{m,tk}^{coa}$ and $\tau_{n,rk}^{coa}$ can be constructed via

$$\hat{\tau}_{m,tk}^{coa} = \frac{2\pi}{\lambda}\left(\hat{r}_{m,tk}^{coa} - \hat{r}_{tk}^{coa}\right) \tag{25}$$

$$\hat{\tau}_{n,rk}^{coa} = \frac{2\pi}{\lambda}\left(\hat{r}_{n,rk}^{coa} - \hat{r}_{rk}^{coa}\right). \tag{26}$$

Using $\hat{\tau}_{m,tk}^{coa}$ and $\hat{\tau}_{n,rk}^{coa}$ as references, the unambiguous estimates for $\tau_{m,tk}$ and $\tau_{n,rk}$ can be obtained via

$$\hat{\tau}_{m,tk}^{fin} = \underset{m_t}{argmin}\left|\tau_{m,tk}^{coa} - \angle\hat{q}_{m,tk} - 2\pi m_t\right| \tag{27}$$

$$\hat{\tau}_{n,rk}^{fin} = \underset{n_r}{argmin}\left|\tau_{n,rk}^{coa} - \angle\hat{q}_{n,rk} - 2\pi n_r\right|. \tag{28}$$

Then, by rearranging (6) and (7), two overdetermined linear equations can be formed as follows

$$\underbrace{\begin{bmatrix} 2\left(\frac{\hat{\tau}_{-M,tk}^{fin}}{2\pi/\lambda}\right) & 2d_{-M,t} \\ \vdots & \vdots \\ 2\left(\frac{\hat{\tau}_{-1,tk}^{fin}}{2\pi/\lambda}\right) & 2d_{-1,t} \\ 2\left(\frac{\hat{\tau}_{1,tk}^{fin}}{2\pi/\lambda}\right) & 2d_{1,t} \\ \vdots & \vdots \\ 2\left(\frac{\hat{\tau}_{M,tk}^{fin}}{2\pi/\lambda}\right) & 2d_{M,t} \end{bmatrix}}_{\mathbf{H}_{t,k}} \underbrace{\begin{bmatrix} r_{tk} \\ r_{tk}\sin\theta_{tk} \end{bmatrix}}_{\mathbf{\Gamma}_{t,k}} = \underbrace{\begin{bmatrix} (d_{-M,t})^2 - \left(\frac{\hat{\tau}_{-M,tk}^{fin}}{2\pi/\lambda}\right)^2 \\ \vdots \\ (d_{-1,t})^2 - \left(\frac{\hat{\tau}_{-1,tk}^{fin}}{2\pi/\lambda}\right)^2 \\ (d_{1,t})^2 - \left(\frac{\hat{\tau}_{1,tk}^{fin}}{2\pi/\lambda}\right)^2 \\ \vdots \\ (d_{M,t})^2 - \left(\frac{\hat{\tau}_{M,tk}^{fin}}{2\pi/\lambda}\right)^2 \end{bmatrix}}_{\mathbf{T}_{t,k}} \tag{29}$$

$$\underbrace{\begin{bmatrix} 2\left(\frac{\hat{\tau}_{-N,rk}^{fin}}{2\pi/\lambda}\right) & -2d_{-N,r} \\ \vdots & \vdots \\ 2\left(\frac{\hat{\tau}_{-1,rk}^{fin}}{2\pi/\lambda}\right) & -2d_{-1,r} \\ 2\left(\frac{\hat{\tau}_{1,rk}^{fin}}{2\pi/\lambda}\right) & -2d_{1,r} \\ \vdots & \vdots \\ 2\left(\frac{\hat{\tau}_{N,rk}^{fin}}{2\pi/\lambda}\right) & -2d_{N,r} \end{bmatrix}}_{\mathbf{H}_{r,k}} \underbrace{\begin{bmatrix} r_{rk} \\ r_{rk}\sin\theta_{rk} \end{bmatrix}}_{\mathbf{\Gamma}_{r,k}} = \underbrace{\begin{bmatrix} (d_{-N,r})^2 - \left(\frac{\hat{\tau}_{-N,rk}^{fin}}{2\pi/\lambda}\right)^2 \\ \vdots \\ (d_{-1,r})^2 - \left(\frac{\hat{\tau}_{-1,rk}^{fin}}{2\pi/\lambda}\right)^2 \\ (d_{1,r})^2 - \left(\frac{\hat{\tau}_{1,rk}^{fin}}{2\pi/\lambda}\right)^2 \\ \vdots \\ (d_{N,r})^2 - \left(\frac{\hat{\tau}_{N,rk}^{fin}}{2\pi/\lambda}\right)^2 \end{bmatrix}}_{\mathbf{T}_{r,k}}. \quad (30)$$

By exploiting the LS method, $\mathbf{\Gamma}_{t,k}$ and $\mathbf{\Gamma}_{r,k}$ can be solved as

$$\hat{\mathbf{\Gamma}}_{t,k} = \left(\mathbf{H}_{t,k}^H \mathbf{H}_{t,k}\right)^{-1} \mathbf{H}_{t,k}^H \mathbf{T}_{t,k} \quad (31)$$

$$\hat{\mathbf{\Gamma}}_{r,k} = \left(\mathbf{H}_{r,k}^H \mathbf{H}_{r,k}\right)^{-1} \mathbf{H}_{r,k}^H \mathbf{T}_{r,k}. \quad (32)$$

Therefore, the fine estimates of 4-D parameters can be calculated as

$$\begin{cases} r_{tk}^{fin} = \hat{\mathbf{\Gamma}}_{t,k}(1) \\ \hat{\theta}_{tk}^{fin} = \sin^{-1}\left(\hat{\mathbf{\Gamma}}_{t,k}(2)/\hat{\mathbf{\Gamma}}_{t,k}(1)\right) \end{cases} \quad (33)$$

$$\begin{cases} r_{rk}^{fin} = \hat{\mathbf{\Gamma}}_{r,k}(1) \\ \hat{\theta}_{rk}^{fin} = \sin^{-1}\left(\hat{\mathbf{\Gamma}}_{r,k}(2)/\hat{\mathbf{\Gamma}}_{r,k}(1)\right) \end{cases}. \quad (34)$$

4. Algorithm Analysis

4.1. Algorithm Summary

The main steps of the proposed algorithm are summarized in Tab. 1.

Table 1: Steps of the Proposed Algorithm.

Step	Operation
Step 1	According to Eqs. (13), (15) and (17), the estimates of $\mathbf{A}_t$, $\mathbf{A}_r$ and $\mathbf{S}$ are updated iteratively until converge, and finally the estimates of $\hat{\mathbf{A}}_t$ and $\hat{\mathbf{A}}_r$ are obtained.
Step 2	Obtain $\hat{\theta}_{m,tk}$ and $\hat{\theta}_{n,rk}$ via Eq. (19) and Eq. (21), respectively, and further obtain $\hat{\theta}_{tk}^{coa}$, $\hat{\theta}_{rk}^{coa}$, r_{tk}^{coa} and r_{rk}^{coa}.
Step 3	Compute $\hat{q}_{m,tk}$ and $\hat{q}_{n,rk}$ via Eq. (23) and Eq. (24).
Step 4	Construct $\hat{\tau}_{m,tk}^{coa}$ and $\hat{\tau}_{n,rk}^{coa}$ according to Eq. (25) and Eq. (26), and then obtain $\hat{\tau}_{m,tk}^{fin}$ and $\hat{\tau}_{n,rk}^{fin}$.
Step 5	Employ the LS method to solve Eq. (29) and Eq. (30), and finally get $\hat{\theta}_{tk}^{fin}$, $\hat{\theta}_{rk}^{fin}$, r_{tk}^{fin} and r_{rk}^{fin}.

4.2. Deterministic CRB

To derive the deterministic Cramr-Rao Bound (CRB) for the estimates of DOD, RFTT, DOA and RFTR, first, define a real-valued vector of unknown parameters as $\mathbf{\Theta} = [\boldsymbol{\theta}_t^T, \boldsymbol{\theta}_r^T, \mathbf{r}_t^T, \mathbf{r}_r^T]^T$ with $\boldsymbol{\theta}_t = [\theta_{t1}, \theta_{t2}, \cdots, \theta_{tK}]^T$, $\boldsymbol{\theta}_r = [\theta_{r1}, \theta_{r2}, \cdots, \theta_{rK}]^T$, $\mathbf{r}_t = [r_{t1}, r_{t2}, \cdots, r_{tK}]^T$, and $\mathbf{r}_r = [r_{r1}, r_{r2}, \cdots, r_{rK}]^T$. Then, the (p, q)th entry of the $4K \times 4K$ CRB matrix for the parameters in $\mathbf{\Theta}$ is given by [16–18]

$$[\mathbf{CRB}^{-1}(\mathbf{\Theta})]_{p,q} = \frac{2L}{\sigma_n^2} Re\left\{ \frac{\partial \mathbf{A}^H}{\partial \mathbf{\Theta}_p} \mathbf{P}_{\mathbf{A}}^{\perp} \frac{\partial \mathbf{A}}{\partial \mathbf{\Theta}_q} \mathbf{R}_S \right\} \tag{35}$$

where $\mathbf{A} = \mathbf{A}_t \odot \mathbf{A}_r$, $\mathbf{P}_{\mathbf{A}}^{\perp} = \mathbf{I}_{4(2M+1)(2N+1)} - \mathbf{A}(\mathbf{A}^H\mathbf{A})^{-1}\mathbf{A}^H$, $\mathbf{R}_S = \frac{1}{L}\mathbf{S}^H\mathbf{S}$.

Define

$$\tilde{\mathbf{A}} = [\mathbf{A}_{\theta_t}, \mathbf{A}_{\theta_r}, \mathbf{A}_{r_t}, \mathbf{A}_{r_r}] \tag{36}$$

with $\mathbf{A}_{\theta_t} = \left[\frac{\partial \mathbf{A}}{\partial \theta_{t1}}, \cdots, \frac{\partial \mathbf{A}}{\partial \theta_{tK}}\right]$, $\mathbf{A}_{\theta_r} = \left[\frac{\partial \mathbf{A}}{\partial \theta_{r1}}, \cdots, \frac{\partial \mathbf{A}}{\partial \theta_{rK}}\right]$, $\mathbf{A}_{r_t} = \left[\frac{\partial \mathbf{A}}{\partial r_{t1}}, \cdots, \frac{\partial \mathbf{A}}{\partial r_{tK}}\right]$, $\mathbf{A}_{r_r} = \left[\frac{\partial \mathbf{A}}{\partial r_{r1}}, \cdots, \frac{\partial \mathbf{A}}{\partial r_{rK}}\right]$, and after some simplification, the closed-form expression for the CRB is given by

$$\mathbf{CRB}(\mathbf{\Theta}) = \frac{\sigma_n^2}{2L}\left\{ Re\left[\left(\tilde{\mathbf{A}}^H \mathbf{P}_{\mathbf{A}}^{\perp} \tilde{\mathbf{A}} \right) \oplus \left(\mathbf{1}_4 \otimes \mathbf{1}_4^T \otimes \mathbf{R}_S^T \right) \right] \right\}^{-1}. \tag{37}$$

4.3. Computational Complexity

The main computational complexity of the proposed method is reflected in step 1 (Trilinear Decomposition), and its complexity is denoted as $O(2(2M+1)K^2 + 2(2N+1)K^2 + LK^2)$, while the computational costs for

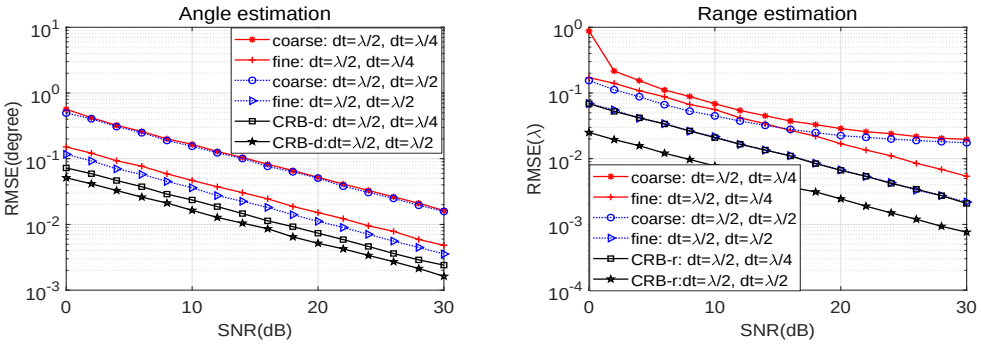

(a) Angle estimation (b) Range estimation

Figure 2: Estimation performance under different receive elements spacing.

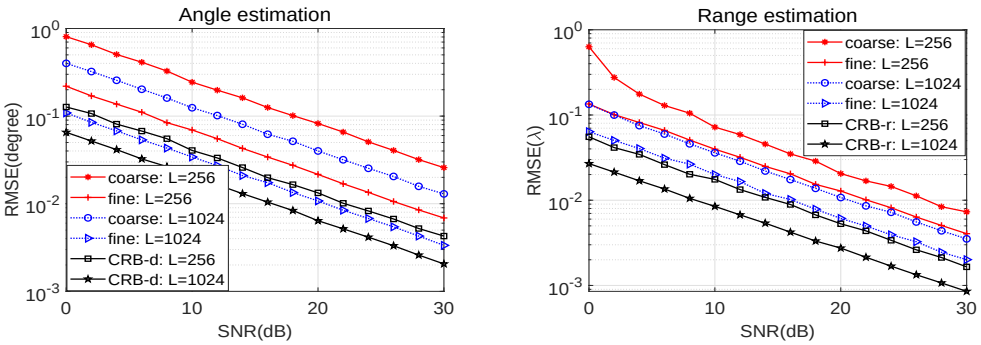

(a) Angle estimation (b) Range estimation

Figure 3: Estimation performance under different number of snapshots.

steps. 2, 3, 4 and 5 are negligible compared with step 1.

5. Simulation Results

In this section, performance of the proposed algorithm is assessed through a series of simulations. First, assume that the source signals are narrowband and uncorrelated, and there are two targets in the NF space, with 4-D parameters $(\theta_{tk}, \theta_{rk}, r_{tk}, r_{rk})$ being $(60°, 45°, 3.5\lambda, 5\lambda)$ and $(45°, 50°, 2\lambda, 3\lambda)$, respectively. Unless otherwise stated, assume that $M = N = 3$, $L = 512$ and the inter-element spacings in the transmitting array and the receiving array are $\lambda/2$.

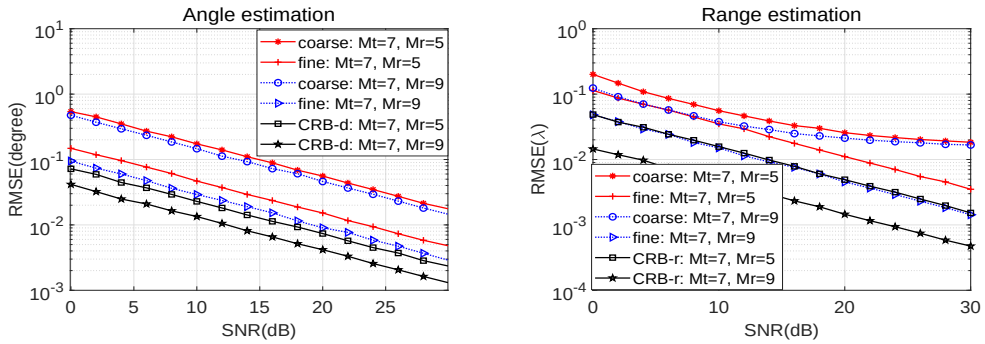

(a) Angle estimation

(b) Range estimation

Figure 4: Estimation performance under different number of receive sensors.

The estimation performance is evaluated through the root-mean-square error (RMSE) defined as $RMSE = \sqrt{\frac{1}{500K}\sum_{k=1}^{K}\sum_{p=1}^{500}\left(\hat{\vartheta}_{p,k} - \vartheta_k\right)^2}$, where $\hat{\vartheta}_{p,k}$ denotes the estimate of the parameters θ_{tk}, r_{tk}, θ_{rk}, r_{rk} at the pth Monte-Carlo trial, and ϑ_k represents the true value. In addition, CRB-d in the legend refers to the average CRB of DOD and DOA, while CRB-r in the

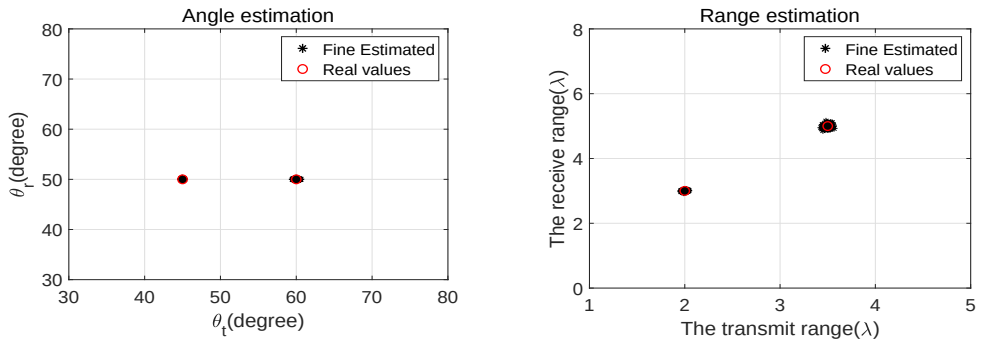

(a) Angle estimation (b) Range estimation

Figure 5: Estimation results of two targets with identical DOA; SNR=10dB, L=200, and 200 independent trials are performed.

legend refers to the average CRB of RFTT and RFTR.

In the first simulation, the performance of the proposed algorithm is examined in terms of the coarse and fine estimates with signal-to-noise ratio (SNR) varying from 0dB to 30dB under different array element spacings. It can be seen from Fig. 2(a) that when the transmitting array element spacing is the same, the angle RMSE obtained by fine estimation decreases significantly with the increase of receiving array element spacing, while that obtained by coarse estimation does not change significantly. This is because the coarse estimates of DOA obtained by Eq. (21) are independent of array element spacing, and thus, they are not sensitive to its change. As for the range estimate in Fig. 2(b), the RMSE obtained by fine estimation is smaller than that by coarse estimation. In addition, when the receiving array element spacing is different, the RMSE of angle and range parameters obtained by both decreases with the increase of the receiving array element spacing.

The same conclusion can be drawn for the transmitting array, which is not shown here to avoid unnecessary repetition

In the second simulation, the performance of the proposed algorithm is studied under different number of snapshots (L), and the other parameters are the same as before. Fig. 3 (a) and Fig. 3 (b) show the angle and range estimation results, where it can be clearly observed that when the number of snapshots is the same, the RMSE of both angle and range obtained by the fine estimation is smaller than that obtained by the coarse estimation. Moreover, when the number of snapshots is different, the RMSE of the coarse estimation and the fine estimation decreases significantly with increase of the number of snapshots, which in turn improves the time diversity gain.

Fig. 4 (a) and (b) present the performance with a varying number of receiving sensors, and the other settings are the same as the first simulation. It can be seen that when the number of transmitting sensors is the same, the RMSE of angle estimate and range estimate obtained by coarse estimation and fine estimation decreases significantly with the increase of the receiving sensors. The same conclusion can be drawn for the number of transmitting elements.

In the last simulation, ability of the proposed method to handle the angle (for example, DOA) ambiguity [19, 20] problem is demonstrated with two targets. As shown in Fig. 5, the proposed method can accurately estimate the 4-D parameters of the two targets with identical DOAs. Actually, targets with 1-D ambiguity such as identical DODs, RFTT or RFTR can be identified effectively without any pairing issue by the proposed method.

6. Conclusions

In this paper, a 4-D parameter estimation method for a bistatic MIMO system has been proposed, where both the transmitter and the receiver are equipped with velocity vector sensor arrays. The 4-D parameters can be automatically paired and accurately estimated through trilinear decomposition, avoiding the extra parameter pairing process and spectrum peak search. In addition, the inter-element spacing does not need to be limited to a quarter wavelength. As indicated by numerical simulations, the proposed method has a good estimation performance, which is close to the derived CRB.

Acknowledgement

This work was supported by the Zhejiang Provincial Natural Science Foundation of China under Grant LY23F010003, by the National Natural Science Foundation of China under Grants 62001256, 62222109 and 61871282, by the Zhejiang Provincial Natural Science Foundation of China (Distinguished Young) under Grant LR20F010001, and by Key Laboratory of Intelligent Perception and Advanced Control of State Ethnic Affairs Commission under grant MD-IPAC-2019102, and the UK Engineering and Physical Sciences Research Council (EPSRC) under grants EP/T517215/1 and EP/V009419/1, and by the Scientific Research Foundation of Graduate School of Ningbo University under grant IF2022130.

References

[1] A. Abdi, H. Guo, A new compact multichannel receiver for underwater wireless communication networks, IEEE Transactions on Wireless Com-

munications 8 (7) (2009) 3326–3329. doi:10.1109/TWC.2009.070566.

[2] J. He, M. N. S. Swamy, M. O. Ahmad, Joint space-time parameter estimation for underwater communication channels with velocity vector sensor arrays, IEEE Transactions on Wireless Communications 11 (11) (2012) 3869–3877. doi:10.1109/TWC.2012.092112.110875.

[3] A. Gunes, M. B. Guldogan, Joint underwater target detection and tracking with the bernoulli filter using an acoustic vector sensor, Digital Signal Processing 48 (2016) 246–258. doi:https://doi.org/10.1016/j.dsp.2015.09.020.

[4] K. Wu, V. G. Reju, A. W. H. Khong, Multisource DOA estimation in a reverberant environment using a single acoustic vector sensor, IEEE/ACM Transactions on Audio, Speech, and Language Processing 26 (10) (2018) 1848–1859. doi:10.1109/TASLP.2018.2845121.

[5] M. Aktas, H. Ozkan, Acoustic direction finding using single acoustic vector sensor under high reverberation, Digital Signal Processing 75 (2018) 56–70. doi:https://doi.org/10.1016/j.dsp.2018.01.001.

[6] A. Nehorai, E. Paldi, Acoustic vector-sensor array processing, IEEE Transactions on Signal Processing 42 (9) (1994) 2481–2491. doi:10.1109/78.317869.

[7] J. He, M. N. S. Swamy, M. O. Ahmad, Joint DOD and DOA estimation for MIMO array with velocity receive sensors, IEEE Signal Processing Letters 18 (7) (2011) 399–402. doi:10.1109/LSP.2011.2152393.

[8] J. Li, X. Zhang, Improved joint DOD and DOA estimation for MIMO array with velocity receive sensors, IEEE Signal Processing Letters 18 (12) (2011) 717–720. doi:10.1109/LSP.2011.2171948.

[9] J. Li, D. Jiang, F. Wang, DOA estimation for sparse nested MIMO radar with velocity receive sensor array, Multidimensional systems and signal processing 29 (2018) 1397–1410.

[10] T. Shu, J. He, V. Dakulagi, 3-D near-field source localization using a spatially spread acoustic vector sensor, IEEE Transactions on Aerospace and Electronic Systems 58 (1) (2022) 180–188. doi:10.1109/TAES.2021.3092703.

[11] V. N. Hari, A. B. Premkumar, X. Zhong, A decoupled approach for near-field source localization using a single acoustic vector sensor, Circuits Systems Signal Processing 32 (2) (2013) 843–859.

[12] Y. Song, K. T. Wong, Three-dimensional localization of a near-field emitter of unknown spectrum, using an acoustic vector sensor corrupted by additive noise of unknown spectrum, IEEE Transactions on Aerospace and Electronic Systems 49 (2) (2013) 1035–1041. doi:10.1109/TAES.2013.6494397.

[13] Z. Jiang, H. Chen, W. Liu, G. Wang, 3-D temporal-spatial-based near-field source localization considering amplitude attenuation, Signal Processing 201 (2022) 108735. doi:https://doi.org/10.1016/j.sigpro.2022.108735.

[14] J. He, T. Shu, L. Li, T.-K. Truong, Mixed near-field and far-field localization and array calibration with partly calibrated arrays, IEEE Transactions on Signal Processing 70 (2022) 2105–2118. doi:10.1109/TSP.2022.3168975.

[15] N. D. Sidiropoulos, R. Bro, On the uniqueness of multilinear decomposition of N-way arrays, Journal of Chemometrics 14 (3) (2015) 229–239.

[16] F. Wen, J. Shi, G. Gui, H. Gacanin, O. A. Dobre, 3-D positioning method for anonymous UAV based on Bistatic polarized MIMO radar, IEEE Internet of Things Journal 10 (1) (2023) 815–827. doi:10.1109/JIOT.2022.3204267.

[17] J. He, M. N. S. Swamy, M. O. Ahmad, Efficient application of MUSIC algorithm under the coexistence of far-field and near-field sources, IEEE Transactions on Signal Processing 60 (4) (2012) 2066–2070. doi:10.1109/TSP.2011.2180902.

[18] H. Chen, W. Wang, W. Liu, Joint DOA, range, and polarization estimation for rectilinear sources with a COLD array, IEEE Wireless Communications Letters 8 (5) (2019) 1398–1401. doi:10.1109/LWC.2019.2919542.

[19] F. Wen, G. Gui, H. Gacanin, H. Sari, Compressive sampling framework for 2D-DOA and polarization estimation in mmwave polarized massive MIMO systems, IEEE Transactions on Wireless Communications (2022) 1–1doi:10.1109/TWC.2022.3215965.

[20] H. Chen, C. Hou, W.-P. Zhu, W. Liu, Y.-Y. Dong, Z. Peng, Q. Wang, Esprit-like two-dimensional direction finding for

mixed circular and strictly noncircular sources based on joint diagonalization, Signal Processing 141 (2017) 48–56. doi:https://doi.org/10.1016/j.sigpro.2017.05.024.